

Optimal interconnection of three-terminal tandem solar cells

Henning Schulte-Huxel¹  | Robert Witteck^{1,2} | Susanne Blankemeyer¹ | Marc Köntges¹

¹Institute for Solar Energy Research Hamelin (ISFH), Emmerthal, Germany

²National Renewable Energy Laboratory (NREL), Golden, CO, USA

Correspondence

Henning Schulte-Huxel, Institute for Solar Energy Research Hamelin (ISFH), Am Ohrberg 1, Emmerthal 31860, Germany.
Email: schulte-huxel@isfh.de

Funding information

U.S. Department of Energy (Office of Science, Office of Basic Energy Sciences and Energy Efficiency and Renewable Energy, Solar Energy Technology Program), Grant/Award Number: SETP DE-EE00038266; Deutsche Forschungsgemeinschaft, Grant/Award Number: SCHU 3206/1-1; German Federal Ministry for Economic Affairs and Climate Action, Grant/Award Number: 03EE1056A

Abstract

Three-terminal (3T) tandem solar cells require an adapted module integration scheme in order to explore their full efficiency potential. The three terminals allow to extract the power of the top and bottom cell separately. In a cell string, the wide bandgap top cells are interconnected in parallel to multiple bottom cells resulting in a parallel/series interconnection. This interconnection scheme affects the operation of the subcells, the resulting current path between the subcells, the layout of the cell interconnects, and the system level. Here, we analyze by simulations and experiments the aspects of the module integration of series- and reverse-connected 3T cells with their practical impact on module processes and performance as well as the effect of varying voltage ratios on the string-end losses. If the subcells are connected in series, the module integration requires insulation layers and significantly longer interconnects compared to devices with reverse-connected subcells. Tandem devices with a reverse connection and a voltage ratio between top and bottom cell of 2:1 allow a lean interconnection design and low integration losses. We present an approach for the integration of bypass diodes for the protection against shading effects that allow to minimize string-end and shading losses for a system of modules featuring 3T cells.

KEYWORDS

module interconnection, multijunction solar cells, PV module, Si-based tandem solar cells

1 | INTRODUCTION

Tandem solar cells with Si bottom cells have drawn high interest in the recent years since they allow to raise the efficiency of conventional single junction Si solar cells.^{1–3} The easiest way to integrate tandem devices into a module is a stack of two series-connected subcells with two terminals (2T)^{4,5} and to interconnect them in series similar to conventional solar cells. This is done by connecting the rear contact of one cell to the front contact of an adjacent cell. This results in a cell string with two contacts as illustrated in Figure 1A, which can be integrated in a conventional manner. Due to the series interconnection of the subcells, this approach requires their current matching. As a consequence, the band gaps of the subcells have to be optimized with respect to each other and the specific operation conditions. This can

be challenging for outdoor operations with varying irradiation spectra,^{5–8} different environmental conditions, or different degradation rates for the subcells. This constraint can be avoided by contacting the two subcells separately, resulting in devices with four terminals (4T); see Figure 1B. For stacked tandem, this requires two (additional) conductive layers to contact the junctions individually, which comes along with its optical and electrical losses,^{9,10} and the separate processing of the subcells and subcell strings.

As an alternative, three-terminal (3T) devices have been developed⁵ and fabricated.^{11,12} A common third terminal enables the power extraction of the individual subcells and allows the 3T cells to perform as good as or even better than 4T devices.^{10,13} Furthermore, the internal interconnection of top and bottom subcell is done monolithically as for 2T tandems without the need of an additional transparent lateral conductive layer. Most research on 3T tandem devices focuses on cell level; however, several aspects have to be considered

Henning Schulte-Huxel and Robert Witteck contributed equally.

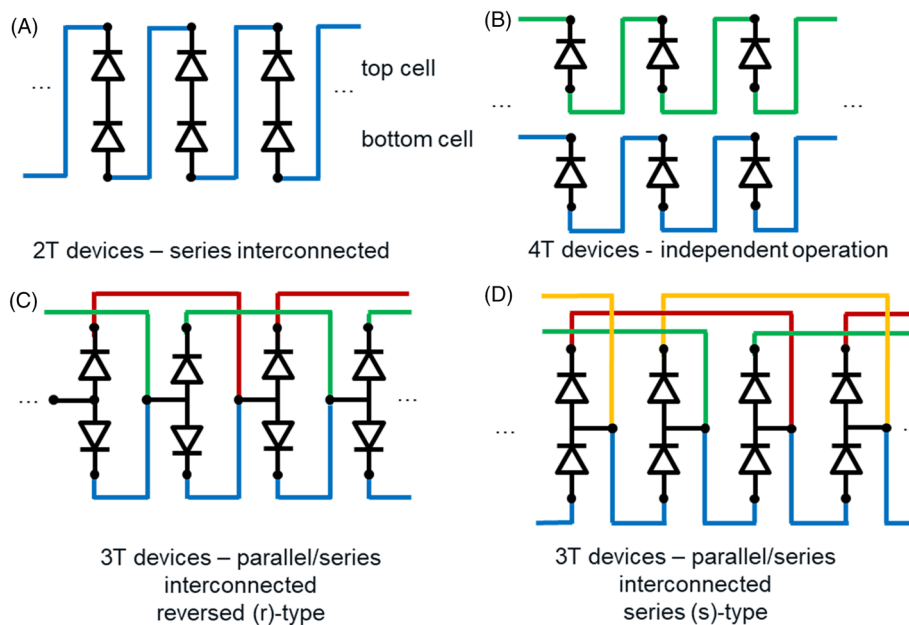


FIGURE 1 Illustration of interconnection schemes of (A) two-terminal (2T), (B) four-terminal (4T), (C) r-type three-terminal (3T), and (D) s-type 3T devices. For the 3T devices, a voltage ratio of top to bottom cell of 2:1 is assumed. The schematics only show the middle sections of a string. Colored edges show the parallel paths within the string. [Colour figure can be viewed at wileyonlinelibrary.com]

when integrating the devices into modules and photovoltaic (PV) systems.

Three-terminal devices can be fabricated in various forms, which can be grouped with respect to the relative orientation of the p-n-junctions of the subcells.¹⁴ A device with a tunnel or recombination junction, where both diodes have the same orientation with respect to their polarity and are connected in series, is called s-type 3T device (see Figure 1D). In contrast, a device with a carrier-selective ohmic contact layer and a reversed diode orientation with respect to their polarity is called r-type 3T tandem device (see Figure 1C). Figure 1C,D shows the module integration of r- and s-type 3T cells, respectively. n top cells in series are interconnected in parallel to m bottom cells in series, where m and n are integers.^{5,6,15} Thereby, the voltage of the top and the bottom cells, V_{top} and V_{bot} , are constrained to a voltage ratio of $V_{\text{top}}/V_{\text{bot}} = m/n$. This requires a voltage-matching of the subcells, where the ratio m/n is defined by the chosen module integration. This constrains the voltage and reduces the efficiency compared to an independent operation.^{5-7,16} However, the losses due to non-optimal bandgap combinations or changing illumination spectra^{5-7,16} are smaller for 3T devices than for 2T devices as the currents of the subcells can vary independently. Due to the logarithmic dependence of voltage on the illumination intensity, a voltage matched 3T tandem has a higher robustness against spectral variation than a current matched 2T device.^{5-7,16} This leads to an overall higher energy yield also when including temperature effects.^{6,16-18} Furthermore, it allows in case of 3T cell strings that the current ratio of the top and bottom cell can vary without high energy yield losses.¹⁷ As a consequence, the 3T cell strings can harvest additional light due to bifaciality more efficiently than 2T devices, which allows an increase in energy yield.

The interconnection scheme of, for example, one top cell in parallel to two bottom cells requires to contact the terminals of a 3T device not only to its nearest neighbor but also to its second-nearest neighbor (see Figure 1C,D). The latter is however missing at the string ends

leading to power losses in the order of at least one 3T device as described in Gee⁵ and McMahon et al.¹⁵ The string-end losses vary with the number of series- and parallel-interconnected cells as well as the subcell configuration, that is, whether the subcells are series or reverse connected.

Apart from the fundamental string-end losses for r- and s-type cells as well as the various string voltage-matching configurations, several aspects of the practical module integration have not been addressed in the literature so far. Therefore, this work analyzes the practical module integration of 3T cells in dependence on the cell configuration. We focus on 2:1 voltage-matched devices as they generally result in the lowest string-end losses.^{5,15} We present an interconnection design based on back-contact solar cells and analyze the string interconnection complexity in terms of cell wiring. Furthermore, we analyze the string-end losses with regard to non-ideally voltage-matched subcells from the substring up to the system level. Moreover, we present for the first time a bypass diode concept for a string with 3T cells to mitigate partial-shading losses and reverse-bias damage.

2 | MODEL PARAMETERS AND EXPERIMENTAL VERIFICATION

2.1 | Cell design

In this study, we focus on the r- and s-type cell configuration with a voltage ratio for the top cell voltage V_{top} and the bottom cell voltage V_{bot} of 2:1, that is, $V_{\text{top}} = 2 \times V_{\text{bot}}$, when interconnected in the cell string. A typical material combination for monolithic devices allowing for such a voltage ratio is for instance a perovskite/silicon tandem.¹² Voltage ratios based on higher integers are less favorable for different reasons^{5,6,15} as will be discussed in the following. Figure 2 shows both cell configurations with (a) showing the r-type and (b) showing

the s-type configuration, respectively. For the cell architecture, we consider an interdigitated back contacted (IBC) bottom cell with a full-area top cell.¹⁹ Thus, the rear side of the tandem device features the root (R) and common (Z) contacts and the front side features the top (T) contact.¹⁴ This architecture has the advantage that it does not require a lateral conducting contact in-between the subcells for the Z contact, which would result in additional optical and electrical losses.

2.2 | Cell parameters

For our simulation study on the string-end losses, we consider a perovskite (PSC) top and silicon bottom cell as tandem cell application scenario. Our model is based on the measurement parameters given in Gharibzadeh et al.²⁰ We employ a single-diode model (SDM) implemented in LTspiceXVII and re-model the reference values within a

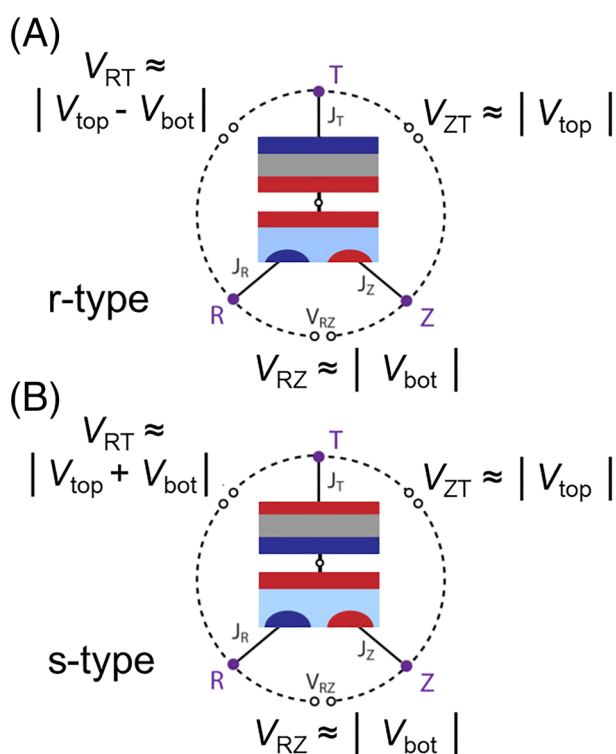


FIGURE 2 Voltage between the three terminals of a 3T solar cell with (A) showing the r-type and (B) showing the s-type configuration. The nomenclature and images are adapted from Warren et al.¹⁴ [Colour figure can be viewed at wileyonlinelibrary.com]

TABLE 1 Parameters of a single-diode model to reproduce the *JV*-parameters of the perovskite top and silicon bottom cell reported in Gharibzadeh et al.²⁰ and the resulting conversion efficiencies η .

	J_{sc} (mA/cm ²)	J_{01} (fA/cm ²)	R_s (Ω cm ²)	R_{sh} (k Ω cm ²)	η (%)	FF (%)	V_{oc} (V)
Top cell	19.85	9.22×10^{-7}	7.7402	10	17.4	76.7	1.14
Bottom cell	15.6	108.8	1.5471	13.3	8.3	80.6	0.66

Note: In the string-end loss variation, J_{01} of the top cell is a free parameter to simulate the effect of different top and bottom cell voltage-matching ratios and varies from $(9.22 \times 10^{-4}$ to $9.22 \times 10^{-13})$ fA/cm².

deviation of 1% from the measured parameters. As input parameter for the SDM, we employ the short-circuit current density J_{sc} and fit the dark saturation current density J_{01} until our modeled open-circuit voltage V_{oc} matches the one in the reference. Further, we fit the series resistance R_s to match the reported fill factor *FF*. The values are given in Table 1. We vary J_{01} of the top cell in the range from 9.22×10^{-4} fA/cm² to 9.22×10^{-13} fA/cm² to simulate the effect of different voltage ratios between top and bottom cell on the string-end losses. The variation of the J_{01} results in a V_{oc} variation from 0.97 to 1.50 V.

2.3 | String modeling and experimental verification

We use a string of 20 interconnected 3T silicon (Si) solar cells to verify our electrical model for the modeling of string-end losses. The string consists of full and halved Si solar cells only as at the time of writing perovskite solar cells with the dimensions of full-sized silicon solar cells are not available to us. A full Si solar cell emulating the bottom cell is connected in parallel to two in series connected Si half-cells emulating the top cell. The silicon-based top and bottom cells are interconnected in the r-type configuration to emulate a parallel/series interconnection of twenty 3T cells. For the cell interconnection, we employ cell interconnection ribbons (CIR) soldered to the cells' busbars. The CIR of the subcells can be contacted individually between the cells on the rear side of the module to measure the current-voltage (*IV*) characteristics of a string with a varying number of cells. Further, the emulator allows to connect and disconnect the first top and last bottom cell from the circuit, which allows additional measurement configurations to verify the electrical model. For further details on the module and the modeling, we refer to Witteck et al.²¹

3 | CELL INTERCONNECTION DEPENDING ON CELL DESIGN

Figure 1 shows the conceptual string interconnection of 3T cells for the (c) r-type and (d) s-type cell configuration. These cell configurations also result in a different potential difference between the three terminals of the device when operating them under illumination as visualized in Figure 2. In case of the r-type devices, the maximal voltage difference is the voltage across the top cell junction and thus between contacts T and Z. For the s-type devices, the maximal voltage is between contacts T and R and thus the sum of the voltages of

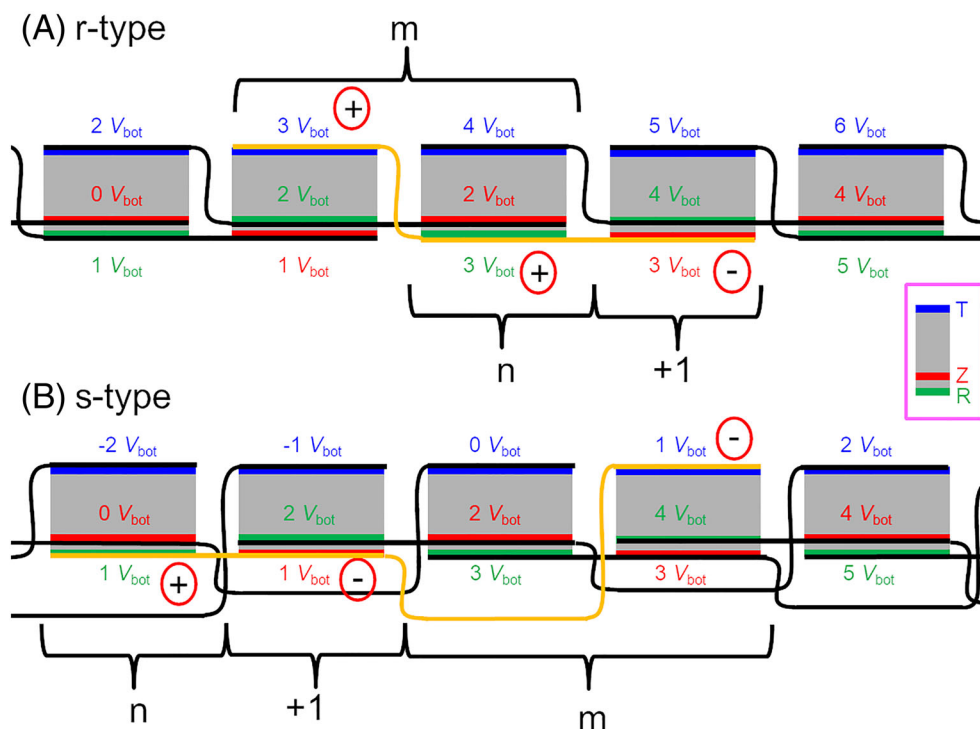


FIGURE 3 Strings of (A) r- and (B) s-type 2:1 3T devices with exemplary orientation of polarities at terminals. Corresponding to the contact naming in Figure 2 it is shown in the magenta inset. The red contact in this figure is the joined contact Z, which is contacted to the green contact R of the bottom and the blue contact T of the top cells through a junction. The interconnects are depicted in black except one contact is in orange to highlight the repeating element. The two contacts of the bottom cell are alternating from cell to cell. For simplicity the bottom cell contacts are depicted above each other. m and n refer to the integer of the voltage ratio $m/n = V_{\text{top}}/V_{\text{bot}}$, here 2:1. [Colour figure can be viewed at wileyonlinelibrary.com]

the top and bottom cell junction. This also has implications for the module integration and results in different cell interconnection for r- and s-type 3TT as will be shown in the following.

Figure 3 shows a two-dimensional representation of the interconnection for the (a) r-type and (b) s-type configuration. The blue-colored front side represents the top contact T of the 3T cells. The red- and green-colored rear sides represent the Z and R contacts of the 3T device, respectively. For simplicity, Figure 3 shows only one busbar per polarity for the 3T cells. Note that in reality, an IBC bottom cell for instance features many busbars on the rear side with alternating polarity. Moreover, the IBC busbar interconnectors are depicted in this two-dimensional representation above each other instead of next to each other.

Starting from the left in Figure 3A, the joined Z contact in red is connected to ground and the voltage difference between the Z and R contact is V_{bot} , the voltage of the bottom cell. The top cell between the blue and red contact has twice the voltage of the bottom cell. The interconnection of the bottom cells is realized analogously to typical IBC cells with busbars, where subsequent cells are positioned to align alternating busbars for each polarity, thus allowing a straight interconnect connecting the cells. The very same interconnect contacting the R and Z contacts of two adjacent cells' rear sides can be used to contact the subsequent cell's front contact T with the same potential; see the orange interconnect in Figure 3A. As the green and blue contact

have the same polarity, they can be interconnected to each other in order to collect their current as already demonstrated in Zehender et al.²² This results in a simple sequence of a front-back interconnection and an IBC interconnection with the same interconnect; thus, it is a combination of two established interconnection processes, one as used for bifacially contacted solar cells and one for rear-contacted solar cells. The front-back interconnection can also be done by other approaches such as shingling, omitting and the need to contact, for example, a pressure sensitive perovskite layer with an interconnect.

In case of an interconnection of s-type devices in Figure 3B, from the perspective of the common Z contacts (red) the T (blue) and the R (green) contact are located in opposite directions. This results in longer interconnects compared to the r-type; see, for example, the orange interconnect in Figure 3A,B. Additional to the 33% longer path, the interconnect must pass one cell without contacting the metallization or the other interconnect, requiring an additional insulation layer on the cell's rear side.

Considering the position of the contact at the same potential with respect to the Z contact, we observe that in case of the r-type devices the interconnect contacting the equipotential R and T contacts leads in the same direction with respect to the Z contact. Therefore, the interconnect connecting the T and the Z contact passes by the R contact and connects it; see Figure 3A. In contrast, for an s-type string, the equipotential contacts are located in opposite directions with

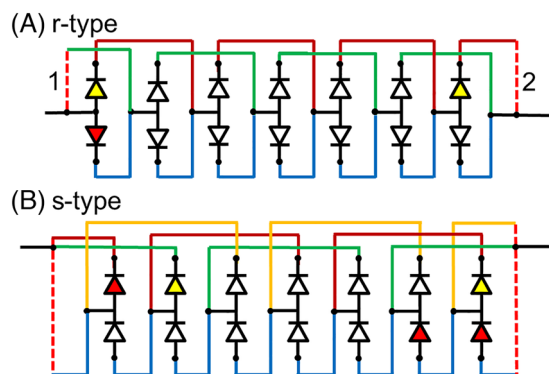


FIGURE 4 Illustration of interconnection schemes in a diode representation for strings of (A) r-type and (B) s-type 3T solar cells. A 2:1 voltage ratio of top to bottom cell is assumed. The red dashed lines are optional connections between the string terminals having a large impact on the overall string power. In case the numbered red dashed connections 1 and 2 are formed, the red cells (representing a single diode) deliver no power to the string and the yellow cells about half their power. [Colour figure can be viewed at [wileyonlinelibrary.com](https://onlinelibrary.wiley.com)]

respect to the Z contact. Thus, the interconnect between T and Z contact needs to be extended and to skip one cell. The length of the interconnects is proportional to the integers from the voltage ratio $m/n = V_{\text{top}}/V_{\text{bot}}$, as shown in Figure 3. This results in the following length of the interconnect L_{ic} for a linear interconnection of the 3T cells with a voltage ratio of m/n :

$$L_{ic} \approx \begin{cases} [\max(m, n)+1] \cdot L_{cell} & \text{for r-type (1a)} \\ (m+n+1) \cdot L_{cell} & \text{for s-type (1b)} \end{cases} \quad (1)$$

where L_{cell} is the length of one cell in string direction. As the interconnect has also to contact the Z contact, this results in the +1 term. For simplicity, we ignore the cell gap and the distance between the end of the interconnect to the cell edge. For the interconnection of 2T devices, the interconnect length would be twice L_{cell} . Consequently, an r-type string and an s-type of 3:2 voltage-matched 3T cells results in a total length of the interconnects of about four and six times the cell length, respectively. As the cells have three contacts, for the s-type devices, the three other interconnects must pass the cell without contacting it. This causes additional efforts for insulation as well as costs and series resistance contributions due the long interconnects. Thus, for 3:2 s-type 3T devices, linear interconnection schemes are not feasible and matrix approaches²³ in combination with multi-layer conductive back sheets may offer a (expensive) alternative.

4 | EFFECTS AT ENDS OF STRINGS

Figure 4A shows a string of 3T cells in r-type configuration for a voltage ratio of 2:1 for the top and bottom cells in a simple diode representation. The string ends on the left- and right-hand side have two terminals on different voltage levels. The connections in Figure 4A are

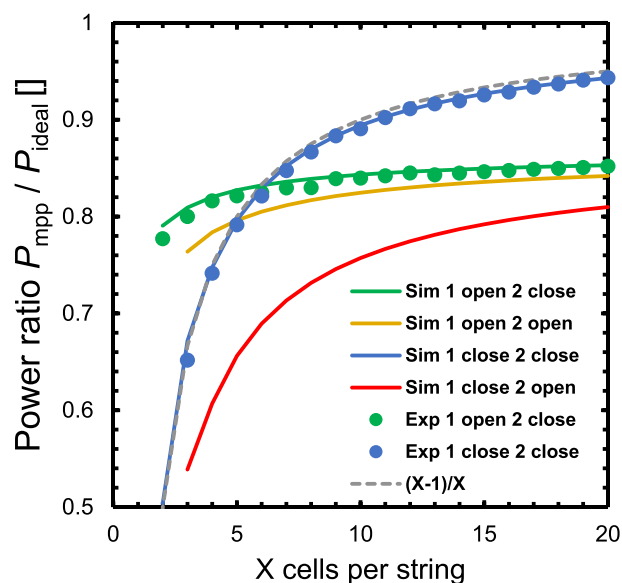


FIGURE 5 Measured (symbols) and simulated (solid lines) power at the maximum power point (MPP) of the string P_{mpp} is divided by the sum of the individual cell MPP powers P_{ideal} . The green and blue symbols show the experimental results for the cases when the left bottom cell is connected to or disconnected from the string. The simulated results are given for all four combinations of open or closed connections 1 and 2 in Figure 4. The dashed grey line corresponds to the loss of one cell per string with X cells according to Equation 2a. [Colour figure can be viewed at [wileyonlinelibrary.com](https://onlinelibrary.wiley.com)]

numbered with 1 and 2 to reference in the following the option to include or exclude the connections. In general, power electronics are connected to the string ends with one terminal per polarity. As they are all on different potential levels, joining the string ends into one terminal results in a partial voltage loss, as the first and last top cells are only in parallel to one bottom cell. Further, the bottom cell at the left string end will be shortened by joining the black and green contact with connection 1. Alternatively, one could omit connections 1 and 2 at the left- and right-hand side.

We measure the effect of different string-end configurations for a varying string length with our Si 3T emulator module. These measurements help in understanding the effect of different string-end configuration on the string-end losses and to verify the electrical model. The blue and green symbols in Figure 5 show our measurement results for the cases when the left bottom cell is operated in short circuit and not delivering power to the string (connection 1 closed) or included in the string (connection 1 open), respectively. Note that disconnecting the left bottom cell and operating it in open circuit yields a similar result. The measured power at the maximum power point (MPP) of the string P_{mpp} is divided by the sum of the individual cell MPP powers P_{ideal} . Hence, the graph also shows the string-end losses as a function of the string length.

When leaving connection 1 open, the very left bottom cell is included in the string, and the left top cell is connected in parallel to two bottom cells. This situation results in higher power for short strings with up to six cells due to the higher voltage by including the

left bottom cell (green symbols) compared to the case, where the left bottom cell is disconnected from the string (blue symbols). However, the current for the second top and bottom cells from the left-hand side will be limited by the current through the very left bottom cell. This limits the current of the whole string, and thus, for strings with more than six cells, disconnecting the left bottom cell leads to a higher string power than in the case where the string current is limited by the left bottom cell. The number of cells for which it is advantageous to open or close the connection 1 depends on the current that is missing due to the limiting cell at the string ends and the voltage loss when bypassing the left bottom cell. Thus, the turnover point depends on the properties of the subcells and, their specific IV -parameters.

The solid lines in Figure 5 show the simulations with our electrical model. The simulations describe the experimental measurement within the measurement uncertainty. For completeness, also, the effect of the open or closed connection 2 is shown. Out of the four combinations of open or closed contacts 1 and 2, closing 1 and 2 allows the highest power for long strings, since the current of all parallel paths in the center of the string can be transported to the terminal. If one of the two contacts is open, either the first or last bottom cell in the string is limiting the string current. If connection 1 is closed and connection 2 is open, the string has the lowest power as the voltage is reduced by the missing left bottom cell and the current is limited by the right bottom cell. A detailed analysis of the IV curves is given in Witteck et al.²¹

In the preferred combination for longer strings of combining all contacts at the string ends, the current in all parallel paths (blue, dark red, and green) can reach the string's terminals. The left bottom cell (red diode in Figure 4A) is disconnected from the string. The first and last top cells of the string are connected in parallel to their bottom cells to reach the required current of the other cells in the string. However, due to the missing neighboring cells, they operate at about half voltage (yellow diodes). This results in sum in a power loss of about one 3T cell. For the s-type 3T devices with the same voltage matching (VM) ratio in Figure 4B, even two 3T cells are lost in total. We have defined in McMahon et al.¹⁵ a generalized approach approximating the power loss at the string ends $P_{endloss}$:

$$P_{endloss} \approx \begin{cases} [\max(m, n) - 1] * P_{tandem} & \text{for r-type (2a)} \\ (m+n-1) * P_{tandem} & \text{for s-type (2b)} \end{cases} \quad (2)$$

where $m/n = V_{top}/V_{bot}$ is the ratio of the n top cells in parallel to m bottom cells, resulting in the given ratio of their voltages, and P_{tandem} the power of one 3T cell under the given VM condition. All higher m and n values of the voltage ratio result in significantly higher string-end losses, for example, an s-type cell with a low-band-gap perovskite and a voltage ratio of 3:2 results in a power loss of about 4 cells per string. The grey line in Figure 5 corresponds to the loss of one cell per string with X cells $[(X-1)/X]$ according to Equation 2a.

Figure 5 shows the results for an experimental device emulating a string of 3T devices using equal types of cells, here only Si solar cells. This results in almost perfect voltage matching conditions with only small voltage differences at the maximum power point due to resistive

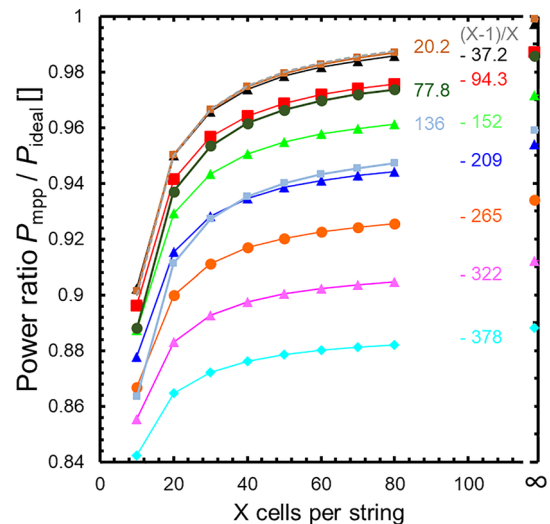


FIGURE 6 Simulated power of the cell string P_{mpp} divided by the power P_{ideal} of the cells in the string when operating the subcells at their individual maximum power points (mpp) for various voltage difference ΔV_{mpp} given in mV by the colored numbers in the plot as a function of the number of cells per string. The dashed gray line corresponds to the loss of one cell per string with X cells according to Equation 2a. Note the interception of the abscissa to indicate the power ratio for an infinite string [Colour figure can be viewed at wileyonlinelibrary.com]

effects. In order to investigate the string-end losses for a realistic device, we adjust our electrical model to the parameters of a perovskite-silicon tandem solar cell. Gharibzadeh et al.²⁰ show that perovskites allow for a tunable band gap, which affects the cell's open-circuit voltage and thus the VM. We fit our single-diode model to the measurement results in Gharibzadeh et al.²⁰ For simplicity, we vary J_{01} in the range from 9.22×10^{-4} fA/cm² to 9.22×10^{-13} fA/cm² to simulate the effect of deviations from the ideal voltage matching. We define this deviation as voltage difference $\Delta V_{mpp} = V_{mpp,top} - 2 \times V_{mpp,bottom}$ to characterize the mismatch between the subcells. $V_{mpp,top}$ and $V_{mpp,bottom}$ are the voltages at MPP when operating the subcells independently.

Figure 6 shows power ratios of the simulated MPP string power P_{mpp} divided by P_{ideal} parameterized by various cell voltage mismatches ΔV_{mpp} given as colored numbers in the figure. Here, we limit our analysis to the r-type case where the last bottom (left bottom cell in Figure 4A) cell is disconnected since this is the most suitable connection for strings longer than six cells. On the right-hand side, the power ratio limited by the voltage mismatch ΔV_{mpp} between one top cell and two bottom cells is shown, which corresponds to an infinite string. It is determined by simulations in which we connect two top cells in parallel to a series of two bottom cells. We simulate the highest string power for a voltage difference close to 0 mV. The power ratio in dependence of the number of cells per string follows again the shape of the limiting case by $[(X-1)/X]$ according to Equation 2a (gray dashed line) shifted by the losses due to the voltage mismatch of the subcells.

Figure 7 shows the superposition of the string-end losses according to Equation 2a and the mismatch losses (dashed lines), that is, $([X-1]/X)$ multiplied by the power of an infinite string, as well as the simulated values (solid lines) for strings of 10 (red) and 80 cells (black). The figure shows an asymmetrical power loss for equal absolute voltage differences $|\Delta V_{\text{mpp}}|$. A positive mismatch, corresponding in the simulated case to a top cell with higher V_{mpp} , leads to higher power losses compared to the same absolute values of the voltage difference $|\Delta V_{\text{mpp}}|$ in the case of a negative mismatch. In case of a negative mismatch, the voltage of the top cell is reduced by increasing J_{01} . This results in a decrease in the fill factor and thus a smaller power loss when deviating from the maximum power point.

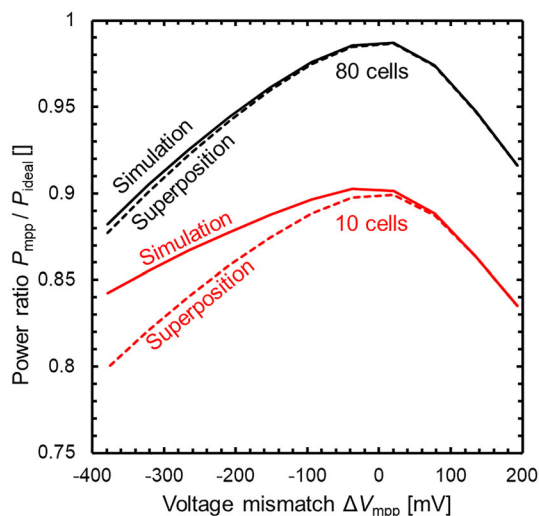


FIGURE 7 Power ratio $P_{\text{mpp}}/P_{\text{ideal}}$ simulated by network simulations (solid lines) in comparison to the superposition of the string end losses according to Equation 2a. In red and black strings of 10 and 80 cells are analyzed, respectively. [Colour figure can be viewed at [wileyonlinelibrary.com](https://onlinelibrary.wiley.com/doi/10.1002/pip.3643)]

Another noticeable aspect in Figure 7 is that the simulated power for the string is higher than the power from the superposition of missing one cell per string (Equation 2) and the voltage mismatch ΔV_{mpp} . The power from the superposition shows a higher power loss than the simulation with negative ΔV_{mpp} . In theory, the last top cells in the string operate at half their voltage and it is assumed that it provides only half of its power, i.e., in total the power of one top cell is lost.¹⁵ As shown in Figure 8 for the case of $\Delta V_{\text{mpp}} = -209$ mV and a string of 20 cells (compare blue curve in Figure 6), the losses of the left and right top cells in the string are less than half of their power. The reason is that they are in parallel to one single bottom cell (second left and right bottom cell, respectively) and forced to lower voltages than their $V_{\text{mpp,top}}$ when they are operated individually. Therefore, their current is increased compared to $I_{\text{mpp,top}}$. Consequently, the current of the bottom cells decreases as well to keep the sum of the currents throughout the string in the parallel paths constant. The latter results in a higher voltage for the top and bottom cells. Thus, the top cells operate at a higher voltage than half its $V_{\text{mpp,top}}$ and at higher currents leading to a higher power than 50% of the cells' power in the center of the string.

When the voltage mismatch is positive and larger, the top cells in the center also operate at voltages lower than their $V_{\text{mpp,top}}$ and at currents higher than their $I_{\text{mpp,top}}$ at independent operation. Thus, shift to smaller voltages for the first and last top cell has small to no effect on its current at that operation point. Additionally, the fill factor of the top cells is larger for higher ΔV_{mpp} and the difference between $I_{\text{mpp,top}}$ and the current at the operation points decreases. Thus, the current gain for the first and last top cell vanishes, and the shift of the operation points to minimize the string end losses decreases compared to the case of negative ΔV_{mpp} .

A negative shift of the operation point allows to reduce the string-end power losses compared to Equation 2a. For example, for $\Delta V_{\text{mpp}} = -209$ mV as in the case of the parameter given in Table 1 and a string of 10 and 80 cells, the power loss is 81% and 82% of the power of a 3T cell. A positive shift of the operation point approaches

10.9	17.5	17.7	17.5	17.7	17.6	17.7	17.6	17.6	17.6	17.6	17.6	17.6	17.6	17.7	17.6	17.7	17.5	17.7	17.5	10.9
0.0	8.3	6.2	8.1	6.5	7.9	6.7	7.7	6.8	7.7	6.8	7.7	6.8	7.7	6.7	7.9	6.5	8.1	6.2	8.3	0.0

FIGURE 8 Top and bottom row show the efficiency in % of the subcells in a cell string of 20 cells for the top and bottom cells, respectively. As input parameters of the single-diode model, we use the values of Table 1. The color code highlights the relative power of the individual cells between 0 (red) and 17.7% (green). [Colour figure can be viewed at [wileyonlinelibrary.com](https://onlinelibrary.wiley.com/doi/10.1002/pip.3643)]

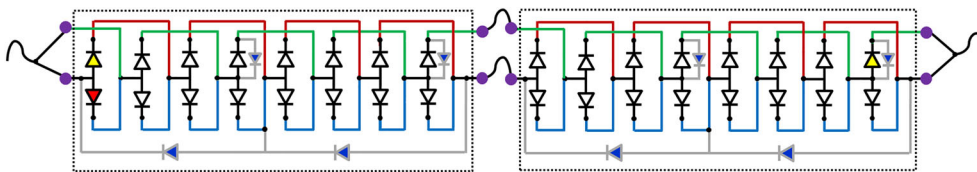


FIGURE 9 Illustration of interconnection schemes in a diode representation for two modules (dashed frames) with two substrings each in the r-type configuration with bypass diodes integrated to protect the module substrings from too large reverse bias. The string-end losses are transferred from substring level to the ends of the module strings. [Colour figure can be viewed at [wileyonlinelibrary.com](https://onlinelibrary.wiley.com/doi/10.1002/pip.3643)]

the theory predicting that 100% of a full tandem cell is lost. For example, for $\Delta V_{\text{mpp}} = 135$ mV and a string of 10 and 80 cells, the power loss is 99.7% and 98.8% of the power of a full tandem cell, respectively. Please note that the shift of the operation point at the string ends causes an alternating pattern of the currents through the top and bottom cells resulting in an alternating pattern of the cell efficiencies within the string; see Figure 8. The extent of the power difference of the alternating pattern decreases with increasing ΔV_{mpp} for the reasons explained above.

5 | STRING END LOSSES ON SYSTEM LEVEL

The presented cell interconnection shows a practical way of creating very long cell strings and thus reduces the string-end losses to a minimum. However, it is known from standard solar modules that long strings carry the risk of reverse-bias problems in case of current mismatch in the string, for example, due to partial shading. In the following, we quantify the string-end losses for PV system of modules with 3T tandem cells and suggest a bypass diode schematic to mitigate reverse-bias-related issues.

We have shown the robustness of r-type strings with 2:1 voltage-matched 3T cells with respect to partial shading due to the parallel current path in Witteck et al.²¹ Nevertheless, a bypass diode is required to protect the cells from too high power dissipation due to reverse bias in case of shading events. One could short circuit the string ends as shown in Figure 4A,B (red dashed lines connections and 2 closed) resulting in string-end losses for each substring in parallel to a bypass diode according to Equation 2a,b. Alternatively, at the system level the substrings could be interconnected by two connections at the string ends allowing to circumvent the issue of the missing neighboring cells and to maintain the periodic parallel connection of one top cell to two bottom cells. Please note that the number of connections is one less than the number of above mentioned parallel paths (Equation 1). So, for an s-type module with a voltage ratio of 3:2, one would need five connections. The interconnection into module strings however requires suitable integration of the bypass diodes to protect the cell strings. The 2:1 r-type configuration allows to integrate a bypass diode in parallel to a continuous string. This allows to shift the string-end loss from the substring level of a module to the end of the module string on system level; see Figure 9. However, due to the parallel current paths, the last top cell in the strings is not protected by the bypass diode in parallel to the string (please note: for all other configurations than 2:1 voltage matched r-type strings, the number of not protected subcells is higher than one cell per string). One option among others is to protect this top cell by an additional bypass diode in parallel to that top cell. In this way, the whole sub-string is protected by two bypass diodes and has two terminals at each string-end allowing an interconnection of the substrings with marginal string-end losses for 2:1 voltage matched strings. Note that the length of the substring protected by the bypass diodes can be adjusted to limit the maximum reverse bias for the tandem cells. A

patent application has been filed for this novel way of interconnection and integration of the bypass diodes.²⁴

Today, a state-of-the-art PV system is usually designed for a system voltage of 1,000 V. Thus, we consider a typical module design for the simulated perovskite-silicon tandem module with 72 cells per module and 20 such modules per inverter to form the PV system. All seventy-two 3T cells in a module are connected in series as well as the 20 modules of the system. Considering the open-circuit voltage of the simulated perovskite-silicon tandem module this results in a PV system voltage of about 950 V. Due to the series interconnection of all substrings and modules, the string-end losses in such a PV system account for 1/1,440 of the power of one r-type 2:1 3T device instead of 1/24 as for the module's substring in a module with 72 cells and 3 bypass diodes. This takes into account another significant advantage of modules with 3T cells: the voltage of a string corresponds to the number of cells times V_{mpp} of the bottom cell (approximating perfect VM) minus the string-end loss according to Equation 2a or b. Adding one tandem cell adds the same voltage as adding one single junction (bottom) cell. In case of 2T devices, adding one cell to the string adds the $V_{\text{mpp,bottom}}$ of the bottom cell plus the $V_{\text{mpp,top}}$ of the top cell, that is, roughly three-times V_{mpp} of the single junction (bottom) cell. This aspect is of high relevance for the interconnection of tandem devices with perovskite top cells being highly sensitive to reverse voltage bias.²⁵ Combined with the fact that in case of partial shading the missing current has to be carried not only by the one shaded top cell, but also to the neighboring parallel top cells (red and green current paths in Figure 9) the voltage drop is distributed over two top cells. Hence, less bypass diodes are required to secure a string of 3T tandems compared to a string with 2T tandem cells.

6 | CONCLUSIONS

From a module perspective, 3T devices and strings come along with significant advantages compared to 2T devices, that is, lower voltages per tandem cell, robustness against spectral mismatch and partial shading. Additionally, compared to 2T tandem cell modules, modules with 3T tandem cell can take full advantage of the absorbed bifacial irradiance as the current of top and bottom cells can be unequal. However, it requires a more complex interconnection scheme which suffers from string-end losses depending on the voltage ratio of the top and bottom cell and their internal connection. Even though for example an s-type interconnection might be beneficial for the processing and performance of individual 3T devices,¹¹ it results for all voltage ratios in significant additional efforts for insulation, costs for the longer interconnects, as well as corresponding series resistance and string-end losses. The most attractive 3T device for module integration is an r-type cell with a voltage ratio of 2:1 due to the lowest string-end losses. Further, we showed in this study a relatively simple interconnection scheme for those devices. This interconnection combines two established interconnection processes, with the one used for bifacially interconnected solar cells and the other for rear-contact solar cells. It requires the lowest wiring length compared to other

voltage ratios or s-type strings, with no need for complex interconnection schemes or insulation.

The string-end losses depend mainly on the cell configuration (r- or s-type) leading to losses corresponding to the power of one or more 3T devices. In this study, we also showed that they are influenced by the properties and the voltage ratio of the subcells. A fraction of the string-end losses can be recovered for cells with low fill factor and in case of voltage-limiting top cells. However, for highly efficient subcells and well-matched voltage combination the partial recovery is only a small fraction of the power of one 3T device. Thus, for long strings, the approximation published in McMahon et al.¹⁵ describes the string-end losses reasonably well.

The upshot of the presented IBC-based interconnection of 3T devices is that it allows the construction of very long strings and to extend the effective string length for the string-end losses to the module or PV system level. This transfers the string-end losses from a substrate to the entire PV system. We quantified the string-end losses for a 1,000 V limited example system consisting of 20 modules each featuring 72 cells with an r-type configuration and voltage ratio of 2:1. Our analysis shows that the string-end loss is only 1/1,440 of the power of a tandem cell. Increasing the system size to e.g. a 1,500 V system will further reduce the string-end losses. We also addressed the reverse-bias problem in case of current mismatch in the event of partially shading such a long string by presenting a novel interconnection scheme employing bypass diodes.

We have shown that the interconnection of 3T devices can be formed by an easy manner and that the losses at the string ends can be minimized in order to benefit from the advantage of 3T tandem solar cells that allow to use broader bandgap combinations of the subcells, higher energy yield and using the full potential of a bifacial application of tandem devices.

ACKNOWLEDGEMENTS

The authors thank Iris Kunze for support of IV measurements of the experimental module, Robby Peibst and Michael Rienäcker for input on 3T cells, and Bianca Lim for discussion and proofreading. This work was supported by the state of Lower Saxony and the 27plus6 project (grant FKZ 03EE1056A) funded by the German Federal Ministry for Economic Affairs and Climate Action. The work of H. Schulte-Huxel was supported by the Research Fellowship by Deutsche Forschungsgemeinschaft Grant SCHU 3206/1-1. This work was authored in part by the National Renewable Energy Laboratory, operated by Alliance for Sustainable Energy, LLC, for the U.S. Department of Energy (DOE) under Contract No. DE-AC36-08GO28308. Robert Witteck acknowledges support by the U.S. Department of Energy's Office of Energy Efficiency and Renewable Energy (EERE) under the Solar Energy Technologies Office Award Number 38266 for the writing and part of the simulations. This report was prepared as an account of work sponsored by an agency of the United States Government. Neither the United States Government nor any agency thereof, nor any of their employees, makes any warranty, express or implied, or assumes any legal liability or responsibility for the accuracy, completeness, or usefulness of any information, apparatus, product, or process disclosed or

represents that its use would not infringe privately owned rights. Reference herein to any specific commercial product, process, or service by trade name, trademark, manufacturer, or otherwise does not necessarily constitute or imply its endorsement, recommendation, or favoring by the United States Government or any agency thereof. The views and opinions of authors expressed herein do not necessarily state or reflect those of the United States Government or any agency thereof.

DATA AVAILABILITY STATEMENT

The data that support the findings of this study are available from the corresponding author upon reasonable request.

ORCID

Henning Schulte-Huxel  <https://orcid.org/0000-0003-4785-0080>

REFERENCES

- Essig S, Allebé C, Remo T, et al. Raising the one-sun conversion efficiency of III-V/Si solar cells to 32.8% for two junctions and 35.9% for three junctions. *Nat Energy*. 2017;2(9):17144. doi:10.1038/nenergy.2017.144
- Rienäcker M, Schnabel M, Warren E, et al. Mechanically stacked dual-junction and triple-junction III-V/Si-IBC cells with efficiencies of 31.5% and 35.4%. 2017. doi:10.4229/EUPVSEC20172017-1AP.1.2.
- Al-Ashouri A, Köhnen E, Li B, et al. Monolithic perovskite/silicon tandem solar cell with 29% efficiency by enhanced hole extraction. *Science*. 2020;370(6522):1300-1309. doi:10.1126/science.abd4016
- Bobela DC, Schmieder KJ, Lumb MP, et al. Demonstration of GaInP₂/Si Voltage Matched Tandem Solar Cells. In: 2017 IEEE 44th Photovoltaic Specialists Conference (PVSC); 25.06.2017–30.06.2017; Washington, DC: IEEE; 25.06.2017–30.06.2017. pp. 2506–2510. doi:10.1109/PVSC.2017.8366407.
- Gee JM. A comparison of different module configurations for multi-band-gap solar cells. *Solar Cells*. 1988;24(1-2):147-155. doi:10.1016/0379-6787(88)90044-0
- Schulte-Huxel H, Friedman DJ, Tamboli AC. String-level modeling of two, three, and four terminal Si-based tandem modules. *IEEE J. Photovoltaics*. 2018;8(5):1370-1375. doi:10.1109/JPHOTOV.2018.2855104
- Trupke T, Würfel P. Improved spectral robustness of triple tandem solar cells by combined series/parallel interconnection. *J Appl Phys*. 2004;96(4):2347-2351. doi:10.1063/1.1766091
- Almansouri I, Ho-Baillie A, Bremner SP, Green MA. Supercharging silicon solar cell performance by means of multijunction concept. *IEEE J. Photovoltaics*. 2015;5(3):968-976. doi:10.1109/JPHOTOV.2015.2395140
- Zhang D, Verhees W, Dörenkämper M, et al. Combination of advanced optical modelling with electrical simulation for performance evaluation of practical 4-terminal perovskite/c-Si tandem modules. *Energy Procedia*. 2016;92:669-677. doi:10.1016/j.egypro.2016.07.039
- Gota F, Langenhorst M, Schmager R, Lehr J, Paetzold UW. Energy yield advantages of three-terminal perovskite-silicon tandem photovoltaics. *Joule*. 2020;4(11):2387-2403. doi:10.1016/j.joule.2020.08.021
- Schnabel M, Schulte-Huxel H, Rienäcker M, et al. Three-terminal III-V/Si tandem solar cells enabled by a transparent conductive adhesive. *Sustainable Energy Fuels*. 2020;4(2):549-558. doi:10.1039/C9SE00893D
- Tockhorn P, Wagner P, Kegelman L, et al. Three-terminal perovskite/silicon tandem solar cells with top and interdigitated rear

- contacts. *ACS Appl Energy Mater.* 2020;3(2):1381-1392. doi:[10.1021/acsaem.9b01800](https://doi.org/10.1021/acsaem.9b01800)
13. Warren EL, Deceglie MG, Rienäcker M, Peibst R, Tamboli AC, Stradins P. Maximizing tandem solar cell power extraction using a three-terminal design. *Sustain Energy Fuels.* 2018;2(6):1141-1147. doi:[10.1039/C8SE00133B](https://doi.org/10.1039/C8SE00133B)
 14. Warren EL, McMahon WE, Rienäcker M, et al. A taxonomy for three-terminal tandem solar cells. *ACS Energy Lett.* 2020;5(4):1233-1242. doi:[10.1021/acseenergylett.0c00068](https://doi.org/10.1021/acseenergylett.0c00068)
 15. McMahon W, Schulte-Huxel H, Buencuerpo J, et al. Homogenous voltage-matched strings using three-terminal tandem solar cells: fundamentals and end losses. *IEEE J Photovoltaics.* 2021;11(4):1078-1086. doi:[10.1109/JPHOTOV.2021.3068325](https://doi.org/10.1109/JPHOTOV.2021.3068325)
 16. Lentine AL, Nielson GN, Okandan M, Cruz-Campa J-L, Tauke-Pedretti A. Voltage matching and optimal cell compositions for microsystem-enabled photovoltaic modules. *IEEE J Photovoltaics.* 2014;4(6):1593-1602. doi:[10.1109/JPHOTOV.2014.2345437](https://doi.org/10.1109/JPHOTOV.2014.2345437)
 17. Schulte-Huxel H, Silverman TJ, Deceglie MG, Friedman DJ, Tamboli AC. Energy yield analysis of multiterminal Si-based tandem solar cells. *IEEE J Photovoltaics.* 2018;8(5):1376-1383. doi:[10.1109/JPHOTOV.2018.2846520](https://doi.org/10.1109/JPHOTOV.2018.2846520)
 18. Liu H, Rodríguez-Gallegos CD, Liu Z, Buonassisi T, Reindl T, Peters IM. A worldwide theoretical comparison of outdoor potential for various silicon-based tandem module architecture. *Cell Reports Physical Science.* 2020;1(4):100037. doi:[10.1016/j.xcrp.2020.100037](https://doi.org/10.1016/j.xcrp.2020.100037)
 19. Nagashima T, Okumura K, Murata K, Kimura Y. Three-terminal tandem solar cells with a back-contact type bottom cell. In: 28th IEEE photovoltaic specialists conference; 15-22 Sept. 2000; Anchorage, AK, USA: IEEE; 2000. pp. 1193-1196. doi: [10.1109/PVSC.2000.916102](https://doi.org/10.1109/PVSC.2000.916102).
 20. Gharibzadeh S, Hossain IM, Fassel P, et al. 2D/3D Heterostructure for semitransparent perovskite solar cells with engineered bandgap enables efficiencies exceeding 25% in four-terminal tandems with silicon and CIGS. *Adv Funct Mater.* 2020;30(19):1909919. doi:[10.1002/adfm.201909919](https://doi.org/10.1002/adfm.201909919)
 21. Witteck R, Blankemeyer S, Siebert M, Köntges M, Schulte-Huxel H. Partial shading of one solar cell in a photovoltaic module with 3-terminal cell interconnection. *Solar Energy Materials and Solar Cells.* 2021;219:110811. doi:[10.1016/j.solmat.2020.110811](https://doi.org/10.1016/j.solmat.2020.110811)
 22. Zehender M, Antolín E, García-Linares P, et al. Module interconnection for the three-terminal heterojunction bipolar transistor solar cell. *AIP Conf Proc.* 2018;2012:40013. doi:[10.1063/1.5053521](https://doi.org/10.1063/1.5053521).
 23. Uzu H, Koizumi G., Solar cell modul, International Patent Application No. PCT/JP2020/012359; 2020.
 24. Schulte-Huxel H, Witteck R, Köntges M. Patent pending: solar modul mit 3-Terminal-Tandem-Solarzellen, German Patent Application No. 10 2022 124 501.2; 2022.
 25. Bowring AR, Bertoluzzi L, O'Regan BC, McGehee MD. Reverse Bias behavior of halide perovskite solar cells. *Adv Energy Mater.* 2018;8(8):1702365. doi:[10.1002/aenm.201702365](https://doi.org/10.1002/aenm.201702365)

How to cite this article: Schulte-Huxel H, Witteck R, Blankemeyer S, Köntges M. Optimal interconnection of three-terminal tandem solar cells. *Prog Photovolt Res Appl.* 2022; 1-10. doi:[10.1002/pip.3643](https://doi.org/10.1002/pip.3643)